ENVIRONMENTAL RESEARCH
LETTERS

LETTER

Rain-fed to irrigation-fed transition of agriculture exacerbates meteorological drought in cropped regions but moderates elsewhere

Sungyoon Kim[1,2], Mukesh Kumar[1,*] and Jonghun Kam[3]

[1] Department of Construction, Civil and Environmental Engineering, University of Alabama, Tuscaloosa, AL, United States of America
[2] Center of Ocean-Land-Atmosphere Studies, George Mason University, Fairfax, VA, United States of America
[3] Division of Environmental Science and Engineering, Pohang University of Science and Technology, Pohang, Republic of Korea
[*] Author to whom any correspondence should be addressed.

E-mail: mkumar4@eng.ua.edu

Keywords: irrigation, land-atmosphere coupling, drought, precipitation

Supplementary material for this article is available online

OPEN ACCESS

RECEIVED
21 October 2022

REVISED
8 June 2023

ACCEPTED FOR PUBLICATION
13 June 2023

PUBLISHED
26 June 2023

Abstract

In recent decades, irrigated agriculture has expanded dramatically over the Southeastern United States (SEUS). The trend is more likely to continue in future given the need to further improve crop productivity and its resilience against droughts, however, the impact of these SEUS land cover changes remains unknown. This study investigates how and to what extent rain-fed to irrigation-fed (RFtoIF) transition in the SEUS region modulates precipitation spatially and temporally under a severe drought meteorological condition. In this study, we perform three Weather Research Forecasting model simulations with varying degrees of irrigated crop areas with meteorological boundary conditions of a record-breaking 2007 drought in the SEUS region. Results show that the SEUS irrigation expansion reduces both the convective triggering potential and low-level humidity index through land-atmospheric interaction. This is accompanied by reduction in the height of atmospheric boundary layer (ABL)-lifting condensation level crossing and increase in the convective available potential energy. These modulations within the ABL provide a favorable condition for strong deep convection during the drought period. However, the impact on precipitation is heterogeneous, with crop areas undergoing RFtoIF transition experiencing an overall reduction in precipitation while other landcovers experiencing an increase. The reduction in precipitation over RFtoIF transitioned croplands is in part due to moisture redistribution aided by generation of an anomalous high-pressure system. The results highlight the complexity of response of precipitation to irrigation expansion in the SEUS, and underscore the need to perform spatially-explicit analysis for mitigating risks to water resources and food security.

1. Introduction

Irrigation continues to expand through the cropped regions all over world to meet the growing demand of food and fiber (Pervez and Brown 2010, Siebert *et al* 2015). Irrigation-fed agriculture already provides for roughly half of the total value of U.S. crop production on 28% of cropland (USDA 2019, Hrozencik and Aillery 2021). Irrigated farmland in the US climbed to 58 million acres in 2017, a 4% increase from 2012 (Nass 2017). In recent decades, significant irrigation expansion has occurred over the humid southeastern US states. For example, irrigated acreage has increased by +46% in Georgia and +212% in Tennessee over 1997–2012 (Walton 2019).

Irrigation expansion can alter a range of coupled environmental states and fluxes. Groundwater pumping for irrigation changes the water table level and base flow (Condon and Maxwell 2019). Its impact on local meteorology has been often studied through the lens of land-atmosphere interactions. Irrigation enhances soil moisture and the water vapor content of

the near-surface, but decreases the surface and near-surface temperature (Sacks *et al* 2009, Ozdogan *et al* 2010, Harding and Snyder 2012, Qian *et al* 2013, Wei *et al* 2013, Lu *et al* 2017). Irrigation expansion modulates the land-atmosphere interactions and other atmospheric processes, resulting in changes in precipitation, however the eventual impacts are oftentimes varied depending on the local hydroclimatic and physiographic conditions (Harding and Snyder 2012). For example, previous studies have reported both deficit or surplus in precipitation due to irrigation (Saeed *et al* 2009, Deangelis *et al* 2010, Puma and Cook 2010, Harding and Snyder 2012, Wei *et al* 2013, Huber *et al* 2014, Pei *et al* 2016).

Given the ongoing rain-fed to irrigation-fed (RFtoIF) transition of croplands in Southeastern United States (SEUS), there is a crucial need to assess how such a RFtoIF transition affects regional precipitation patterns. Specifically, the study aims to better understand the role of irrigation on the land-atmosphere coupling and the modulation of vertical mixing processes and associated large-scale circulations at the sub-seasonal scale during the summer of 2007 when SEUS experienced an extreme meteorological drought. To this end, three Weather Research Forecasting (WRF) model runs for summer (June-August) of 2007 were performed. The WRF model runs consist of a control run with no irrigation on croplands and the two experiment runs with different irrigation expansion perturbations. Through these runs, we answer two scientific questions: (1) how may the RFtoIF transition modulate the land-atmosphere interaction during 2007-like droughts in the SEUS, and (2) will RFtoIF transition impact the precipitation magnitude and pattern over the region? By answering these questions, this study will advance the understanding of the atmospheric response to irrigation expansion.

2. Data, methods, and models

2.1. Study area

The study was conducted for the SEUS states encompassing all of Alabama, Arkansas, Georgia, Louisiana, Mississippi, North Carolina, South Carolina, and Tennessee (figure 1(a)). Some areas of neighboring states were also included. We specifically focus our analysis on the Deep South region that includes Alabama, Georgia, and Mississippi. Notably, despite being a water ample region, the SEUS has experienced severe droughts in recent decades. Over 2006–2008, the SEUS states experienced a severe drought with a peak in 2007, primarily driven by precipitation deficit (Kam *et al* 2014). This drought caused economic losses of over $1 billion and resulted in lack of available water resources along rivers and in lakes, triggering inter-basin water import to the region for the first time in 100 years (Manuel 2008, Campana *et al* 2012). Growing population (PNREAP 2023, USAFacts 2023) and expansion of irrigation-fed agriculture make the regional communities more vulnerable to droughts. There is a need to refine our understanding of whether the anticipated water scarcity risks from meteorological droughts in SEUS will be elevated or suppressed by the indirect impacts of RFtoIF transition on precipitation.

2.2. Experiment design

In this study, Weather Research and Forecasting model version 4 (WRF v4.0) was implemented in the SEUS for the three summer months (June-August) of 2007. The concerned period represents the driest summer during the severest SEUS drought over the last 50 years. The mother and inner model domains discretized the SEUS (domain-01) at 15 km resolution, while the nested Deep South (domain-02) was discretized at 3 km resolution, respectively (figure 1(a)). The inner model domain considers a much-resolved convection-permitting formulation, while the mother model domain uses cumulus physics for computational efficiency (see table S1 for the details of the model configuration).

We used the North American Regional Reanalysis (NARR) dataset (Mesinger *et al* 2006) for initial and lateral boundary conditions of our WRF runs. Default land category data is from the National Land Cover Database (NLCD) of 2006 (Homer *et al* 2020). All cultivated crops and pasture/hay NLCD land categories were defined as croplands for the ensuing analysis. The croplands included both rain-fed and irrigated lands. The irrigation-fed region was selected based on the Moderate Resolution Imaging Spectroradiometer Irrigated Agriculture Datasets for the Conterminous United States (MIrAD-US) Version 4 for 2007 at the 1 km spatial resolution (Shrestha *et al* 2021). We used the Pu-Xleim land surface model (Gilliam and Pleim 2010) that includes shallow (surface to 1 cm) and root-zone (1–99 cm) soil layers.

A spin-up simulation was performed for soil moisture stabilization over May 2007 to generate a more realistic initial soil moisture conditions. To simulate the effects of irrigation, we forced the soil moisture in the 2 soil layers of all irrigated land to be fully saturated during the entire study period. The control (CTL) run was the default WRF simulation where it was assumed that all croplands are rain-fed. For the Experiment 1 (EXP1) run, soil moisture was set to be fully saturated over the irrigation-fed regions. For Experiment 2 (EXP2) run, all croplands, including rain-fed, were assumed to be irrigation-fed. Again, soil moisture was set to full saturation over all irrigation-fed regions. The difference in soil moisture due to RFtoIF transition is well apparent in figures 1(b) and (c).

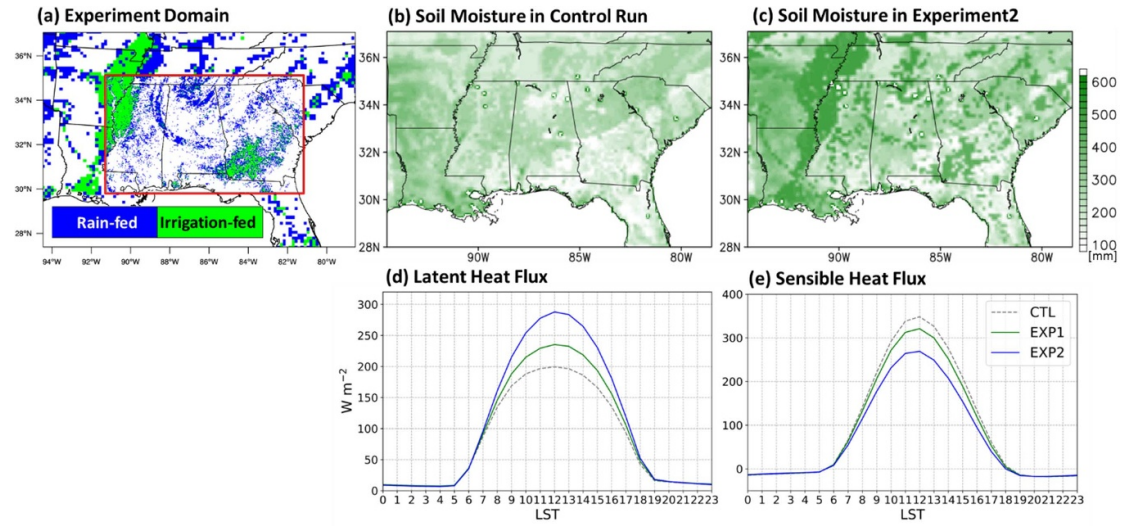

Figure 1. (a) Rain-fed (blue) and irrigation-fed (green) regions in WRF simulations. Frame boundary (grey box) and the red box indicate domain-01 and domain-02, respectively. The 3 month-averaged (from June to August) soil moisture (mm) for (b) rain-fed (control run), and (c) all irrigation-fed (Experiment2) simulations. Spatially-averaged diurnal cycle of (d) latent heat flux (W m^{-2}) and (e) sensible heat flux (W m^{-2}) in domain-02 for Control (CTL), Experiment1 (EXP1), and Experiment2 (EXP2) are shown using grey dots, and green and blue lines, respectively. CTL, EXP1, and EXP2 are WRF simulation configurations where all croplands are considered rain-fed, rain-fed and irrigated-fed distribution of croplands is as per the data in the year 2007, and all croplands are considered irrigation-fed, respectively. LST is local sidereal time.

2.3. Analysis of land-atmosphere coupling

The land-atmosphere coupling was diagnosed via the convective triggering potential (CTP) and low-level humidity index (HI_{LOW}) framework (Findell and Eltahir 2003a, Ferguson and Wood 2011, Jach *et al* 2020, 2022). HI_{LOW} (°C) is calculated by the sum of the dewpoint depressions at 50 and 150 hPa above ground level (AGL) at 6 local sidereal time:

$$HI_{LOW} = (T - T_d)_{AGL-50} + (T - T_d)_{AGL-150}$$

where T and T_d are temperature (°C) and dewpoint temperature (°C), respectively. Subscript of AGL—p indicates the pressure level p AGL. CTP (J kg^{-1}) is obtained by integrating vertical profile between the moist temperature of air parcel, T_m (K) and the environmental temperature, T_e (K) from 100 to 300 hPa AGL at the same time:

$$CTP = g_0 \int_{z_{AGL-300}}^{z_{AGL-100}} \left(\frac{T_m - T_e}{T_e} \right) dz$$

where g_0 is the gravitational acceleration (9.81 m s^{-2}). The height of $z_{AGL-100}$ and $z_{AGL-300}$ are located near 1 km and 3 km, respectively.

The CTP-HI_{LOW} framework classifies land-atmosphere feedback into four categories: (1) dry soil advantage, (2), wet soil advantage, (3) transition and (4) atmospherically controlled. The dry soil advantage regime designates thermal triggering of precipitation wherein high sensible heat flux leads to boundary layer growth and upward mixing of moist air to heights where condensation and formation of rainfall can occur (Dirmeyer *et al* 2014). The wet soil advantage regime specifies hydrologic triggering of precipitation wherein high soil moisture wets the boundary layer thus increasing the predisposition of condensation as the moist air rises. In the transition regime, convection may be triggered in either wet or dry soils. Notably, this configuration seldomly leads to precipitation. The atmospherically controlled regime inhibits the contribution of land towards triggering deep convection. An atmospherically controlled regime may also be termed as 'too dry for rain' and 'too stable for rain'.

3. Results

3.1. Impact of irrigation on land atmosphere interaction

For the summer (June-August) of 2007, the regional averages of simulated monthly 2 m temperature and relative humidity by the three control and experiment WRF runs were evaluated against those from the NARR dataset (supplementary figure S1). The EXP1 run with recent land cover and irrigation area status shows hot and dry bias compared with the NARR data. For example, simulated 2 m temperature in the EXP1 run was slightly overestimated. The EXP1 run underestimated both precipitation (by −0.87 mm d^{-1} or −25.32%) and 2 m RH (by −3.15%). The negative bias of precipitation in the WRF simulation was in line with similar results from previous studies using the WRF model (Prein

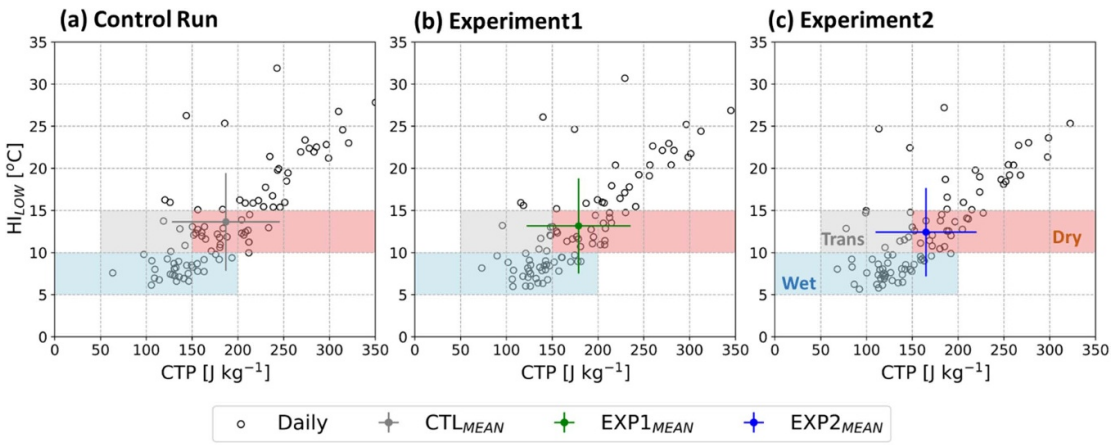

Figure 2. Scatter plot of the spatial average of convective trigger potential (CTP; J kg^{-1}) and low-level humidity index (HI$_{LOW}$; °C), over the Deep South (domain-02) for (a) Control run (CTL; grey), (b) Experiment1 (EXP1; green), and (c) Experiment2 (EXP2; blue). Configuration summary of CTL, EXP1, and EXP2 WRF is presented in figure 1 caption. Each open black dot is a daily average from the simulation. Error bars (in (a)–(c)) denote the one standard deviation of the daily average. Red, blue, and grey rectangles in the background denote regimes of dry soil advantage (Dry), wet soil advantage (Wet), and transition (Trans). White background indicates atmospherically controlled regimes.

et al 2020, Qian *et al* 2020, Shrestha *et al* 2021). Furthermore, the results from the EXP1 run show that a more realistic consideration of irrigation extent reduces the bias at the near surface, which is in line with the findings of previous studies (Qian *et al* 2020, Li *et al* 2022). A cooler and more humid near-surface atmospheric conditions was realized with irrigation expansion in EXP1, which reaffirms the findings from previous studies that irrigation makes the near-surface atmosphere more humid and cooler (Adegoke *et al* 2003, Mahmood *et al* 2006). In the case of full RFtoIF transition of croplands, EXP2 showed further drop in temperature and increase in humidity with respect to EXP1. However the precipitation reduced (more discussion about this is presented in the next section). The expressed response of temperature and humidity with RFtoIF transition is because the latent heat flux in the EXP1 and EXP2 runs were larger than that in CTL (figure 1(d)). More surface cooling from latent heat flux decreased the sensible heat flux in irrigated simulations (figure 1(e)), resulting in more cooling and humidity at the near surface.

Estimates of CTP and HI$_{LOW}$ showed that the averages of CTP-HI$_{LOW}$ in the Deep South were under the dry soil advantage regime during the summer of 2007 (figure 2). It is worth noting that the SEUS region is, however, usually defined as the wet soil advantage regime (Findell and Eltahir 2003b). Furthermore, RFtoIF transition led to a more humid near-surface and more stable atmospheric boundary layer (ABL). For example, the regional averages of HI$_{LOW}$ in EXPs were lower than that in CTL due to a combination of modulation of the surface energy budget (e.g. increased latent heat and decreased sensible heat fluxes). Humid near surface condition also interacted with ABL by making the humid air temperature profile become closer to wet adiabatic. This ABL condition decreased the CTP in EXPs, contributing to a more stable atmospheric condition. With irrigation expansion, the days under the 'atmospherically controlled: too dry for rain' regime (over 15 °C of HI$_{LOW}$) decreased from 33 d in the CTL run to 29 and 22 d in the EXP1 and EXP2 runs, respectively. The days under the 'wet soil advantage' regime, however, increased from 31 d in the CTL run to 35 and 49 d in EXP1 and EXP2 runs, respectively.

3.2. Impact of irrigation on cloud formation and precipitation

Results show that irrigation expansion modulated the vertical distribution of clouds and precipitation via land-atmosphere interactions. Clouds can develop at the height where/when ABL and the lifting condensation level (LCL) intersect. This crossing determines the initiation of cloud formation and convection triggering (Gentine *et al* 2013, Yin *et al* 2015). In the EXP runs, irrigation increased the soil moisture, and consequently the land-atmosphere coupling decreased the height of the ABL-LCL crossing (figure 3(a)). In contrast, the CTL run (drier rain-fed cropland) showed relatively larger sensible heat flux into ABL, consequently deepening the ABL height, which in turn caused a higher ABL-LCL crossing. The difference in height of ABL-LCL crossing vis-à-vis the wetness is consistent with observational (Phillips and Klein 2014) and 1D ideal model (Yin *et al* 2015) studies. Our WRF runs also showed an earlier timing of ABL-LCL crossing for dryer land case

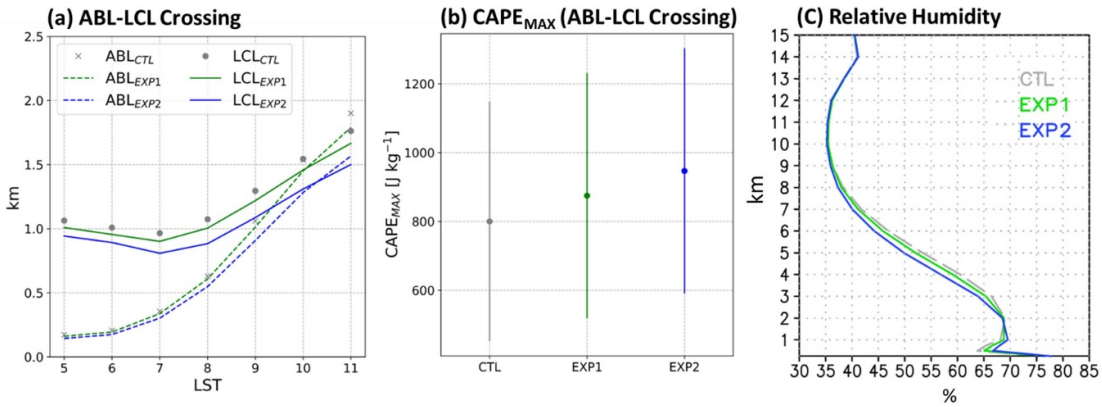

Figure 3. (a) Time evolution of atmospheric boundary layer (ABL; km) height and lifting condensation level (LCL; km) for control (CTL), experiment1 (EXP1), and experiment2 (EXP2) WRF simulations. Configuration summary of CTL, EXP1, and EXP2 is presented in figure 1 caption. ABLs from CTL and EXPs are x marks and dash-dot lines, respectively, while LCLs are shown as filled dots and solid lines. (b) Maximum convective available potential energy (CAPE$_{MAX}$; J kg^{-1}) from CTL, EXP1, and EXP2. Error bars indicate one standard error of spatiotemporal average from runs. (c) Vertical profiles of relative humidity. Grey, green, and blue correspond to CTL, EXP1, and EXP2 runs, respectively. LST is local sidereal time.

that was reported in the previous studies (Phillips and Klein 2014, Yin *et al* 2015). Irrigation-fed simulations showed higher maximum convective available potential energy (CAPE$_{MAX}$) when ABL-LCL crossing occurred (figure 3(b)). It is worth noting that CAPE$_{MAX}$ determines the predisposition of deep convection (Yin *et al* 2015). The spatiotemporal averages of vertical relative humidity showed irrigation expansion in EXP1 and EXP2 resulted in a more humid lower troposphere (figure 3(c)) because of the humid near-surface and lower height of ABL-LCL crossing (Qian *et al* 2013). Overall, these results indicate that irrigation modulated not only the ABL but also the free atmosphere-level condition.

The impact on precipitation is heterogeneous and does not follow the spatial distribution of 2 m temperature, 2 m relative humidity, and soil moisture (supplementary figure S2). For example, the transition from RFtoIF increased soil moisture over the western Mississippi and Tennessee and the southwestern Georgia. However, the spatial pattern of precipitation is much more heterogeneous (figures 4(a) and (b)). Differences between vertically-integrated moisture flux (figures 4(c) and (d)) showed that irrigation transition induced an anomalous high pressure system. The high pressure system became stronger from EXP1 to EXP2 because of enhanced cooling of the land and subsequently the near-surface atmosphere. This high pressure system played a role in altering the spatial distribution of atmospheric moisture, with increased precipitation over parts of Arkansas, Louisiana, and Florida in EXP2. In contrast, moisture fluxes over western South Carolina and croplands of southwestern Georgia impeded the moisture coming in from the eastern shores of the SEUS, resulting in suppressed precipitation. Croplands along the Mississippi River also experienced precipitation suppression due to being near the edge of the anomalous high system. This is of significance as the region is already experiencing groundwater depletion to support irrigated agriculture (Reba *et al* 2017). Further RFtoIF transition in the SEUS may put extra pressure on the groundwater aquifer along the lower Mississippi Basin due to further reduction in precipitation. Overall, the amount of precipitation is found to decrease over croplands but increase over non-cropped areas. The disparity in precipitation between EXP2 and CTL is statistically significant at 5% level based on the two-tailed Student's *t*-test. In terms of the overall atmospheric moisture balance, both crop and non-crop areas experienced a decrease in atmospheric moisture (supplementary figure S3(c)). This is true even though evapotranspiration minus precipitation increased with RFtoIF extent, partially due to increase in evapotranspiration from irrigated cropped areas and also an because of increase in net radiation in non-cropped lands caused by suppressed cloudiness and precipitation conditions resulting from the formation of the high-pressure system (supplementary figure S4). The overall reduction in atmospheric moisture is mainly attributable to a greater divergence of moisture out of the region with increasing extent of RFtoIF transition (supplementary figure S3). This is also consistent with the formation of anomalous high-pressure system in EXP1 and EXP2 (see figure 4). In terms of the total regional precipitation during the summer season, relatively small RFtoIF transition results in an overall enhanced precipitation in the SEUS region, but full RFtoIF transition of all croplands negates the overall increase (supplementary figure S5).

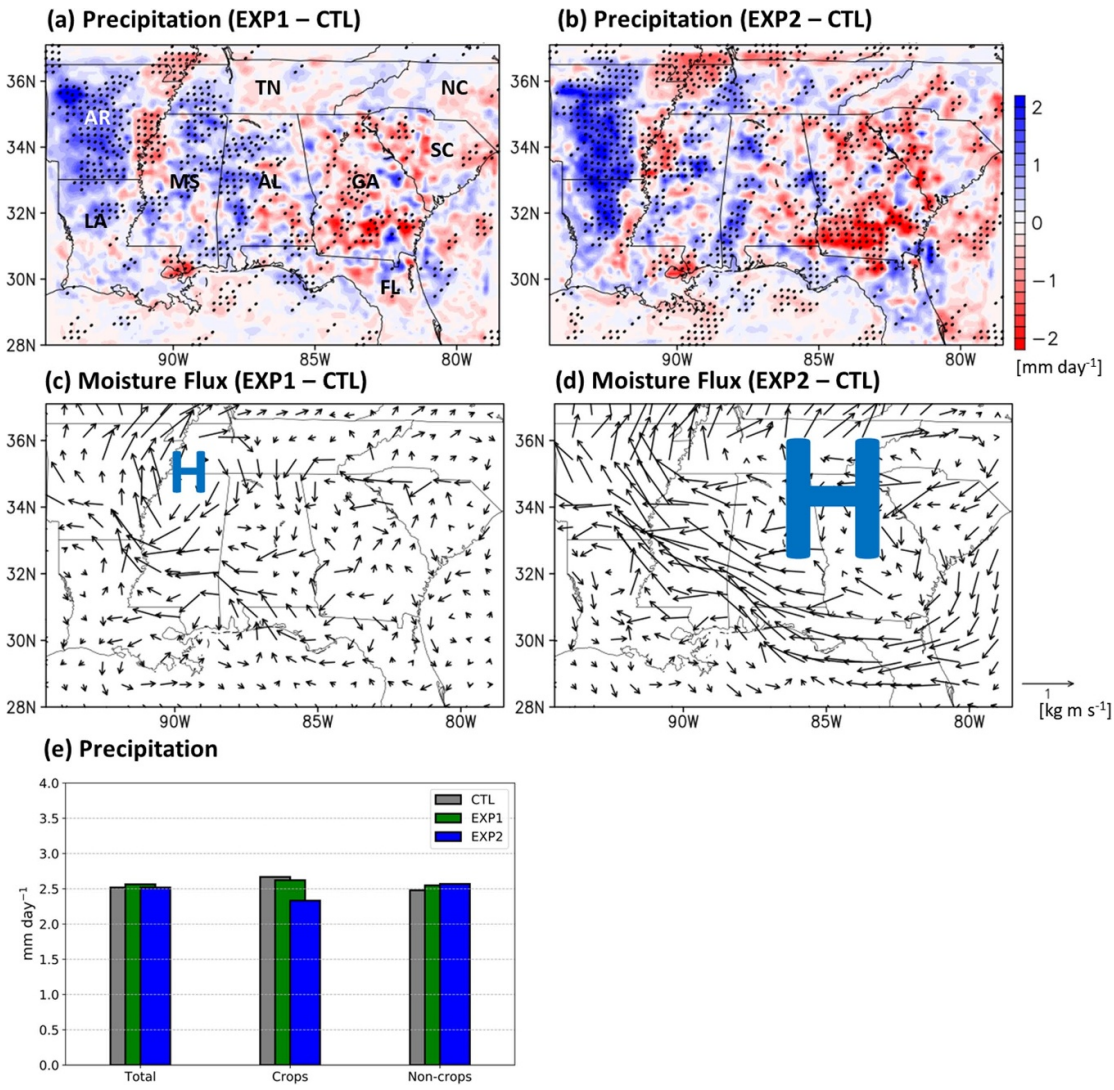

Figure 4. Spatial distribution of average differences for (a), (b) precipitation (mm day^{-1}) and (c), (d) vertically-integrated moisture flux (Q flux, vector; kg m s^{-1}) for EXP1—CTL (left) and EXP2—CTL (right). Configuration summary of CTL, EXP1, and EXP2 is presented in figure 1 caption. The dotted area in (a) and (b) indicates the statistical significance at 5% level from the two-tailed Student's *t*-test. 'H' in (c) and (d) indicate the high-pressure anomalous system. Abbreviations indicate the names of states: Arkansas (AR), Tennessee (TN), North Carolina (NC), South Carolina (SC), Mississippi (MS), Alabama (AL), Georgia (GA), Louisiana (LA), and Florida (FL). (e) The amount of accumulated precipitation (mm day^{-1}) under total, crops, and non-crops fraction area for CTL (grey bars), EXP1 (green bars), and EXP2 (blue bars). Crop area includes both rain-fed and irrigation-fed. The rest of the area is listed as non-crops. The total area equals sum of crops and non-crops.

4. Conclusions and synthesis

Southeastern US has been experiencing RFtoIF transition of agriculture at a faster pace than ever, spurred by a range of socioeconomic impacts including record corn and soybean prices. An amendment in the 2014 US farm bill has also facilitated this expansion by allowing non-western states to apply for federal irrigation grants. The 2007 SEUS drought that caused billions of crop losses, further underscored the need to adjust the level of perceived risk of local stakeholders and policy makers to droughts through irrigation expansion. Through RFtoIF transition, there is a potential for SEUS farmers to increase crop productivity thus yielding economic benefits. Furthermore, the RFtoIF transition would help farmers and insurers manage risks against erratic rainfall, particularly during the dry spells. However, given that RFtoIF transitions and associated modulation of land-atmosphere interaction is likely to affect land-atmosphere coupling, moisture recycling, atmospheric circulation, and precipitation distribution across the scales, assessment of advantages of RFtoIF transition on food and water security, especially during droughts, remain uncertain. This study assessed the impact of RFtoIF transition on modulating precipitation during droughts.

Results showed that irrigation expansion decreased near-surface temperature and increasing nea-surface humidity, which in turn led to reduction

of HI_{LOW} and CTP. In other words, ABL became wetter and more stable. This implies that irrigation weakens dry land-atmosphere coupling in the SEUS region during severe droughts. Despite the smaller potential for convective motion within the ABL, the potential of deep convection was enhanced. However, increased potential of deep convection did not increase precipitation everywhere. The east side of Deep South (e.g. southwestern Georgia) experienced precipitation deficits due to the blocking of moisture transport via anti-cyclone air motions over anomalous near-surface high pressure regions.

Our results were based on a set of WRF simulations. As is the case with most model results, the reported magnitude of the changes has inherent uncertainties. However, the physical consistency of the results between the CTL and EXP runs elicits confidence in their validity. Further confidence in the results could be obtained through the usage of large ensemble members of control and experiment runs, although, the computational demand for such simulations remain prohibitive and will need to be addressed in future studies. In the EXP runs, this study assumed that irrigation was applied in a manner that ensured persistent saturated soil conditions thus minimizing crop stress. Future studies may focus on further elucidating the impacts of different intensities and schedules of irrigation on precipitation alterations.

Despite these limitations, the study demonstrates the impacts of RFtoIF transition in SEUS. Overall, our results imply that, spatially, irrigation expansion may have divergent impacts depending on the area under consideration, with some locations experiencing an increase in precipitation but others (especially cropped regions) experiencing a decrease. The increase is largely due to enhanced source of moisture from irrigation and development of favorable conditions in the lower atmosphere for precipitation occurrence. The decrease is caused by blocking of the moisture flux in the affected regions due to generation of a high-pressure system. The study also highlights a non-monotonic influence on amount of precipitation with RFtoIF transition. In terms of the total precipitation during the summer, relatively small RFtoIF transition (i.e. equivalent to the current irrigated area fraction) results in an overall enhanced precipitation in the region, which can be a welcome change for water users and managers, particularly during a severe drought. However, a full RFtoIF transition, wherein all croplands in the region are transitioned to irrigated land, negates the overall increase due to blocking of incoming moisture flux in the affected areas. The study shows that widespread irrigation expansion may even exacerbate precipitation deficit locally. Given these heterogenous impacts on precipitation, it is important to plan water and food security risk mitigation measures that account for spatially-explicit impacts of regional RFtoIF transitions.

Data availability statement

The data that support the findings of this study are openly available at the following URL/DOI: 10.5281/zenodo.7730157.

Acknowledgments

Mukesh Kumar and Sungyoon Kim acknowledge partial support from NSF (Grant Nos. OIA-2019561 and EAR-1856054) and AL EPSCoR Graduate Research Scholars Program (GRSP), respectively. This work is also made possible in part by high-performance computing resources from NCAR-Wyoming Supercomputing Center (UALT0002 and UALT0005).

Conflict of interest

Authors declare no competing interests.

ORCID iDs

Sungyoon Kim https://orcid.org/0000-0002-3838-7322
Mukesh Kumar https://orcid.org/0000-0001-7114-9978
Jonghun Kam https://orcid.org/0000-0002-7967-7705

References

Adegoke J O, Pielke R A, Eastman J, Mahmood R and Hubbard K G 2003 Impact of irrigation on midsummer surface fluxes and temperature under dry synoptic conditions: a regional atmospheric model study of the US high plains *Mon. Weather Rev.* **131** 556–64

Banacos C and Schultz M 2005 The use of moisture flux convergence in forecasting convective initiation: historical and operational perspectives *Weather Forecast.* **20** 351–66

Campana P, Knox J, Grundstein A and Dowd J 2012 The 2007-2009 drought in Athens, Georgia, United States: a climatological analysis and an assessment of future water availability 1 *J. Am. Water Resour. Assoc.* **48** 379–90

Condon L E and Maxwell R M 2019 Simulating the sensitivity of evapotranspiration and streamflow to large-scale groundwater depletion *Sci. Adv.* **5** eaav4574

Deangelis A, Dominguez F, Fan Y, Robock A, Kustu M D and Robinson D 2010 Evidence of enhanced precipitation due to irrigation over the Great Plains of the United States *J. Geophys. Res.* **115**

Dirmeyer P A, Wang Z, Mbuh M J and Norton H E 2014 Intensified land surface control on boundary layer growth in a changing climate *Geophys. Res. Lett.* **41** 1290–4

Douglas E, Beltrán-przekurat A, Niyogi D, Pielke Sr R and Vörösmarty C 2009 The impact of agricultural intensification and irrigation on land–atmosphere interactions and Indian monsoon precipitation—a mesoscale modeling perspective *Glob. Planet. Change* **67** 117–28

Ferguson C R and Wood E F 2011 Observed land–atmosphere coupling from satellite remote sensing and reanalysis *J. Hydrometeorol.* **12** 1221–54

Findell K L and Eltahir E A 2003a Atmospheric controls on soil moisture–boundary layer interactions. Part I: framework development *J. Hydrometeorol.* **4** 552–69

Findell K L and Eltahir E A 2003b Atmospheric controls on soil moisture–boundary layer interactions. Part II: feedbacks within the continental United States *J. Hydrometeorol.* **4** 570–83

Gentine P, Holtslag A A M, D'andrea F and Ek M 2013 Surface and atmospheric controls on the onset of moist convection over land *J. Hydrometeorol.* **14** 1443–62

Gilliam R C and Pleim J E 2010 Performance assessment of new land surface and planetary boundary layer physics in the WRF-ARW *J. Appl. Meteorol. Climatol.* **49** 760–74

Harding K J and Snyder P K 2012 Modeling the atmospheric response to irrigation in the Great Plains. Part I: general impacts on precipitation and the energy budget *J. Hydrometeorol.* **13** 1667–86

Homer C *et al* 2020 Conterminous United States land cover change patterns 2001–2016 from the 2016 national land cover database *ISPRS J. Photogramm. Remote Sens.* **162** 184–99

Hrozencik R A and Aillery M 2021 Trends in US irrigated agriculture: increasing resilience under water supply scarcity *Economic Information Bulletin* vol 229 (United States Department of Agriculture, Economic Research Service) (https://doi.org/10.2139/ssrn.3996325)

Huber D B, Mechem D B and Brunsell N A 2014 The effects of Great Plains irrigation on the surface energy balance, regional circulation, and precipitation *Climate* **2** 103–28

Jach L, Schwitalla T, Branch O, Warrach-Sagi K and Wulfmeyer V 2022 Sensitivity of land–atmosphere coupling strength to changing atmospheric temperature and moisture over Europe *Earth Syst. Dyn.* **13** 109–32

Jach L, Warrach-Sagi K, Ingwersen J, Kaas E and Wulfmeyer V 2020 Land cover impacts on land-atmosphere coupling strength in climate simulations with WRF over Europe *J. Geophys. Res.* **125** e2019JD031989

KAM J, Sheffield J and Wood E F 2014 A multiscale analysis of drought and pluvial mechanisms for the Southeastern United States *J. Geophys. Res.* **119** 7348–67

Li J, Qian Y, Leung L R, Feng Z, Sarangi C, Liu Y and Yang Z 2022 Impacts of large-scale urbanization and irrigation on summer precipitation in the Mid-Atlantic region of the United States *Geophys. Res. Lett.* **49** e2022GL097845

Lu Y, Harding K and Kueppers L 2017 Irrigation effects on land–atmosphere coupling strength in the United States *J. Clim.* **30** 3671–85

Mahmood R, Foster S A, Keeling T, Hubbard K G, Carlson C and Leeper R 2006 Impacts of irrigation on 20th century temperature in the northern Great Plains *Glob. Planet. Change* **54** 1–18

Manuel J 2008 Drought in the southeast: lessons for water management *Environ. Health Perspect.* **116** A168–71

Mesinger F *et al* 2006 North American regional reanalysis *Bull. Am. Meteorol. Soc.* **87** 343–60

Nass U 2017 Census of agriculture *United States Summary and State Data* (United States Department of Agriculture, National Agriculture Statistics Service)

Ozdogan M, Rodell M, Beaudoing H K and Toll D L 2010 Simulating the effects of irrigation over the United States in a land surface model based on satellite-derived agricultural data *J. Hydrometeorol.* **11** 171–84

Pacific Northwest Regional Economic Analysis Project (PNREAP) 2023 Southeast vs. United States comparative trends report population 1958-2021 (available at: https://united-states.reaproject.org/analysis/comparative-trends-analysis/population/reports/950000/0/)

Pei L, Moore N, Zhong S, Kendall A D, Gao Z and Hyndman D W 2016 Effects of irrigation on summer precipitation over the United States *J. Clim.* **29** 3541–58

Pervez M S and Brown J F 2010 Mapping irrigated lands at 250-m scale by merging MODIS data and national agricultural statistics *Remote Sens.* **2** 2388–412

Phillips T J and Klein S A 2014 Land-atmosphere coupling manifested in warm-season observations on the US southern great plains *J. Geophys. Res.* **119** 509–28

Prein A F, Liu C, Ikeda K, Bullock R, Rasmussen R M, Holland G J and Clark M 2020 Simulating North American mesoscale convective systems with a convection-permitting climate model *Clim. Dyn.* **55** 95–110

Puma M J and Cook B I 2010 Effects of irrigation on global climate during the 20th century *J. Geophys. Res.* **115**

Qian Y, Huang M, Yang B and Berg L K 2013 A modeling study of irrigation effects on surface fluxes and land–air–cloud interactions in the Southern Great Plains *J. Hydrometeorol.* **14** 700–21

Qian Y, Yang Z, Feng Z, Liu Y, Gustafson W I, Berg L K, Huang M, Yang B and Ma H-Y 2020 Neglecting irrigation contributes to the simulated summertime warm-and-dry bias in the central United States *npj Clim. Atmos. Sci.* **3** 31

Reba M L, Massey J H, Adviento-borbe M A, Leslie D, Yaeger M A, Anders M and Farris J 2017 Aquifer depletion in the lower Mississippi river basin: challenges and solutions *J. Contemp. Water Res. Educ.* **162** 128–39

Sacks W J, Cook B I, Buenning N, Levis S and Helkowski J H 2009 Effects of global irrigation on the near-surface climate *Clim. Dyn.* **33** 159–75

Saeed F, Hagemann S and Jacob D 2009 Impact of irrigation on the South Asian summer monsoon *Geophys. Res. Lett.* **36**

Shrestha D, Brown J F, Benedict T D and Howard D M 2021 Exploring the regional dynamics of US irrigated agriculture from 2002 to 2017 *Land* **10** 394

Siebert S, Kummu M, Porkka M, Döll P, Ramankutty N and Scanlon B R 2015 A global data set of the extent of irrigated land from 1900 to 2005 *Hydrol. Earth Syst. Sci.* **19** 1521–45

Siebert S, Webber H, Zhao G and Ewert F 2017 Heat stress is overestimated in climate impact studies for irrigated agriculture *Environ. Res. Lett.* **12** 054023

Thiery W, Davin E L, Lawrence D M, Hirsch A L, Hauser M and Seneviratne S I 2017 Present-day irrigation mitigates heat extremes *J. Geophys. Res.* **122** 1403–22

U.S. Department Of Agriculture Economic Research Service (USDA E) 2019 International agricultural productivity

USAFacts 2023 Our changing population: United States (available at: https://usafacts.org/data/topics/people-society/population-and-demographics/our-changing-population?endDate=2021-01-01&startDate=1991-01-01)

Valmassoi A, Dudhia J, Di Sabatino S and Pilla F 2020 Irrigation impact on precipitation during a heatwave event using WRF-ARW: the summer 2015 po valley case *Atmos. Res.* **241** 104951

Walton B 2019 U.S. irrigation continues steady eastward expansion *Water & Food, Water News, WEF* (available at: www.circleofblue.org/2019/world/u-s-irrigation-continues-steady-eastward-expansion/) (Accessed March 2023)

Wei J, Dirmeyer P A, Wisser D, Bosilovich M G and Mocko D M 2013 Where does the irrigation water go? An estimate of the contribution of irrigation to precipitation using MERRA *J. Hydrometeorol.* **14** 275–89

Yang Q, Huang X and Tang Q 2020 Irrigation cooling effect on land surface temperature across China based on satellite observations *Sci. Total Environ.* **705** 135984

Yang Z, Dominguez F, Zeng X, Hu H, Gupta H and Yang B 2017 Impact of irrigation over the California Central Valley on regional climate *J. Hydrometeorol.* **18** 1341–57

Yin J, Albertson J D, Rigby J R and Porporato A 2015 Land and atmospheric controls on initiation and intensity of moist convection: CAPE dynamics and LCL crossings *Water Resour. Res.* **51** 8476–93

Supporting Information for

Rain-fed to Irrigation-fed Transition of Agriculture Exacerbates Meteorological Drought in Cropped Regions but Moderates Elsewhere

Sungyoon Kim[1, 2], Mukesh Kumar[1], Jonghun Kam[3]

[1]Department of Construction, Civil and Environmental Engineering, University of Alabama, Tuscaloosa, Alabama, United States of America

[2]Center of Ocean-Land-Atmosphere Studies, George Mason University, Fairfax, Virginia, United States of America

[3]Division of Environmental Science and Engineering, Pohang University of Science and Technology, Pohang, Republic of Korea

Submitted to Environmental Research Letters

Supplementary Tables and Figures

Table S1. Physical schemes used in the WRF (v4.0) simulations

Figure S1. Scatter plot of 2 meter temperature and precipitation (left), and 2 meter humidity (right). Each dot is the spatiotemporal average for domain-01 during the 2007 summer season (June-August).

Figure S2. Temporal average of differences in (a-b) 2 meter temperature (°C), (c-d) 2 meter relative humidity (%) and (e-f) soil moisture for EXP1 – CTL (left) and EXP2 – CTL (right). The dotted area denotes the statistical significance at 5% from the two-tailed Student's t-test.

Figure S3. The amount of (a) evapotranspiration (ET) minus precipitation (P) (mm day^{-1}), (b) vertically integrated horizontal moisture flux divergence (mm day^{-1}), and (c) change of atmospheric moisture (mm day^{-1}) over the entire model domain (indicated by total), crop, and non-crop areas for CTL (grey bars), EXP1 (green bars), and EXP2 (blue bars). Crop area includes both rain-fed and irrigation-fed regions. The rest of the land area is non-crops. Divergence in panel (b) indicates flux out of the region. For equations in (b) and (c), g, q, V_h, p, and t indicate the constant of gravitational acceleration, specific humidity, horizontal wind vector, pressure, and time, respectively. Based on Banacos and Schultz (2005), water balance can be written as ET – P + residual = moisture flux divergence + change in atmospheric moisture. Negative residual flux includes vertical divergence out of the region, and errors in flux calculations such as due to the use of a coarser temporal resolution (6 hours) of data variables.

Figure S4. Average net radiation on the surface (W m^{-2}) in different regions.

Figure S5. Time evolution of accumulated precipitation (mm day^{-1}) in summer of 2007. Grey, green, and blue correspond to CTL, EXP1, and EXP2 runs, respectively.

Table S1. Physical schemes used in the WRF (v4.0) simulations

	Domain01	Domain02
Resolution (x grids, y grids)	15 km (107, 74)	3 km (331, 196)
Vertical layers	40	
Cumulus physics	Grell-Devenyi	off
Microphysics	Thompson	
Longwave radiation	RRTMG	
Shortwave radiation	RRTMG	
Planetary boundary layer	ACM2	
Surface layer	Pu-Xleim	
Land surface	Pu-Xleim	

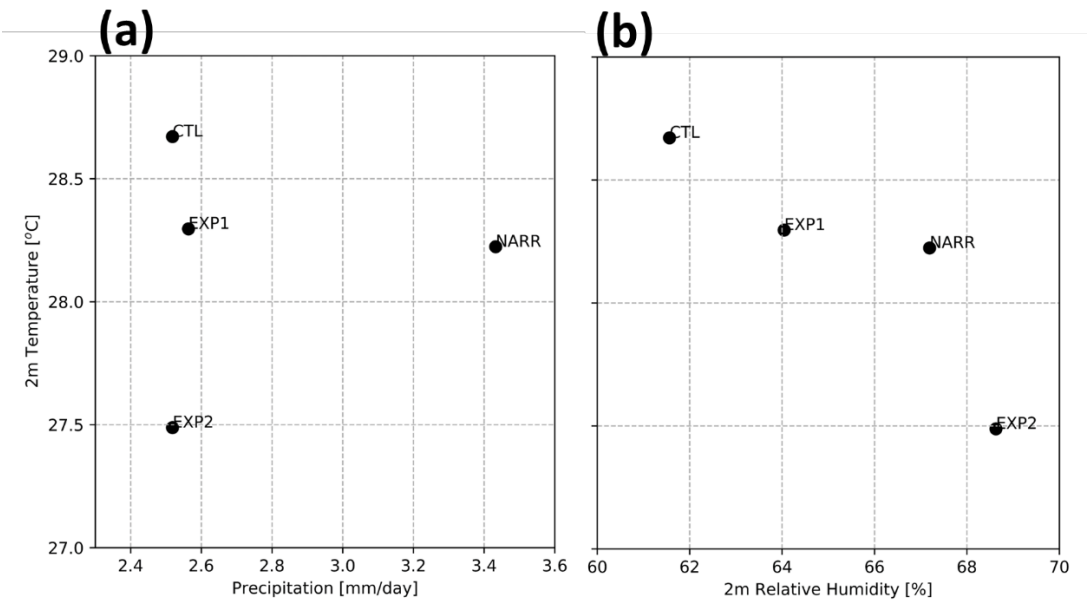

Figure S1. Scatter plot of 2 meter temperature and precipitation (left), and 2 meter humidity (right). Each dot is the spatiotemporal average for domain-01 during the 2007 summer season (June-August).

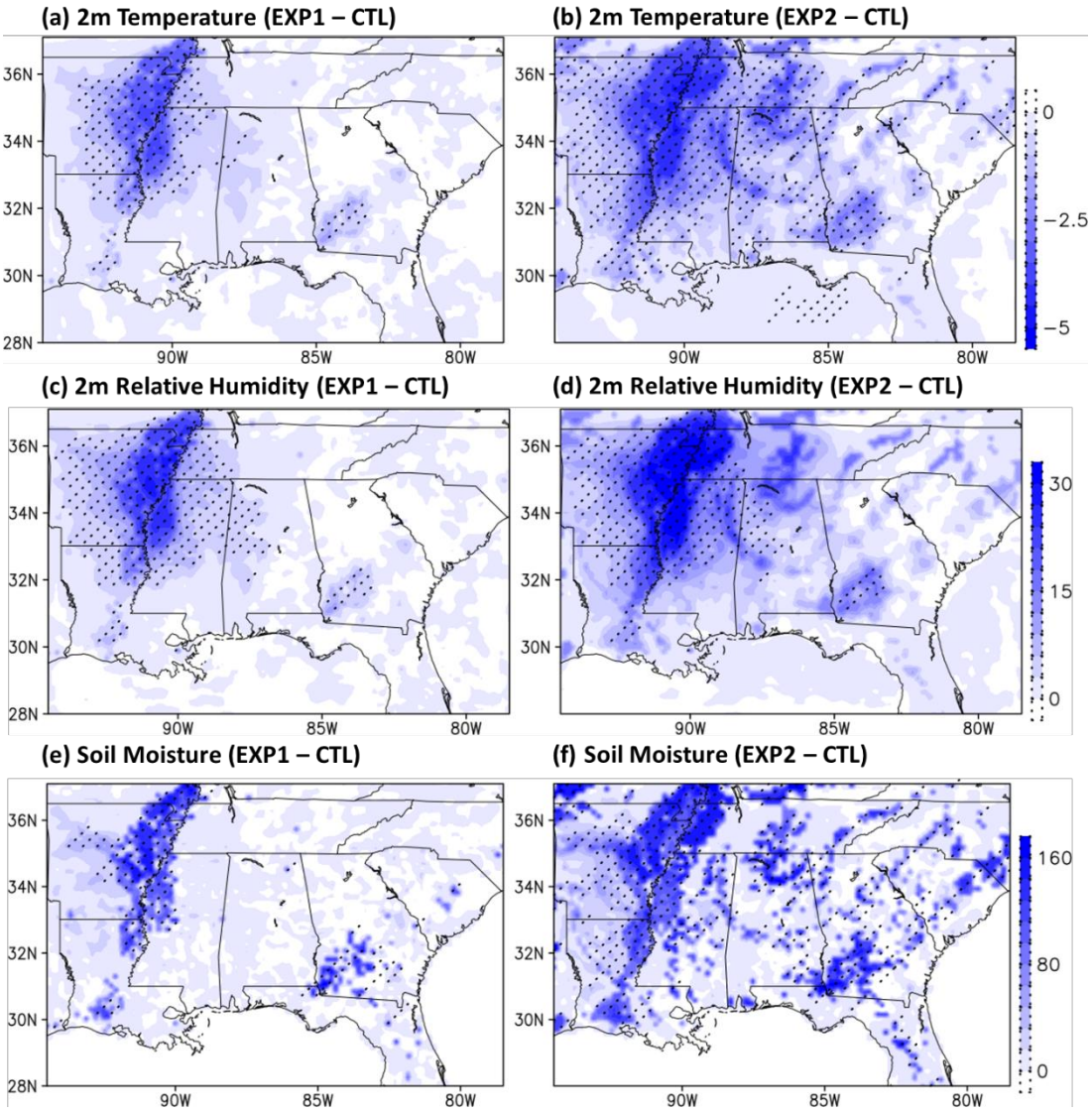

Figure S2. Temporal average of differences in (a-b) 2 meter temperature (°C), (c-d) 2 meter relative humidity (%) and (e-f) soil moisture for EXP1 – CTL (left) and EXP2 – CTL (right). The dotted area denotes the statistical significance at 5% from the two-tailed Student's t-test.

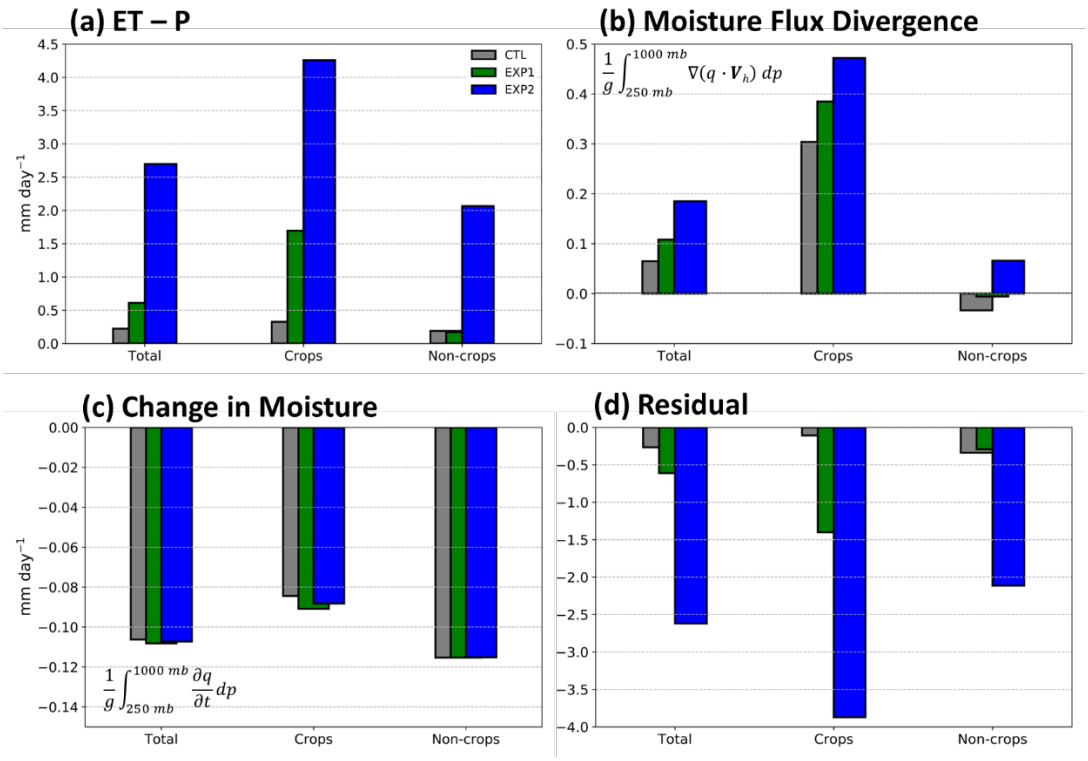

Figure S3. The amount of (a) evapotranspiration (ET) minus precipitation (P) (mm day^{-1}), (b) vertically integrated horizontal moisture flux divergence (mm day^{-1}), and (c) change of atmospheric moisture (mm day^{-1}) over the entire model domain (indicated by total), crop, and non-crop areas for CTL (grey bars), EXP1 (green bars), and EXP2 (blue bars). Crop area includes both rain-fed and irrigation-fed regions. The rest of the land area is non-crops. Divergence in panel (b) indicates flux out of the region. For equations in (b) and (c), g, q, V_h, p, and t indicate the constant of gravitational acceleration, specific humidity, horizontal wind vector, pressure, and time, respectively. Based on Banacos and Schultz (2005), water balance can be written as ET – P + residual = moisture flux divergence + change in atmospheric moisture. Negative residual flux includes vertical divergence out of the region, and errors in flux calculations such as due to the use of a coarser temporal resolution (6 hours) of data variables.

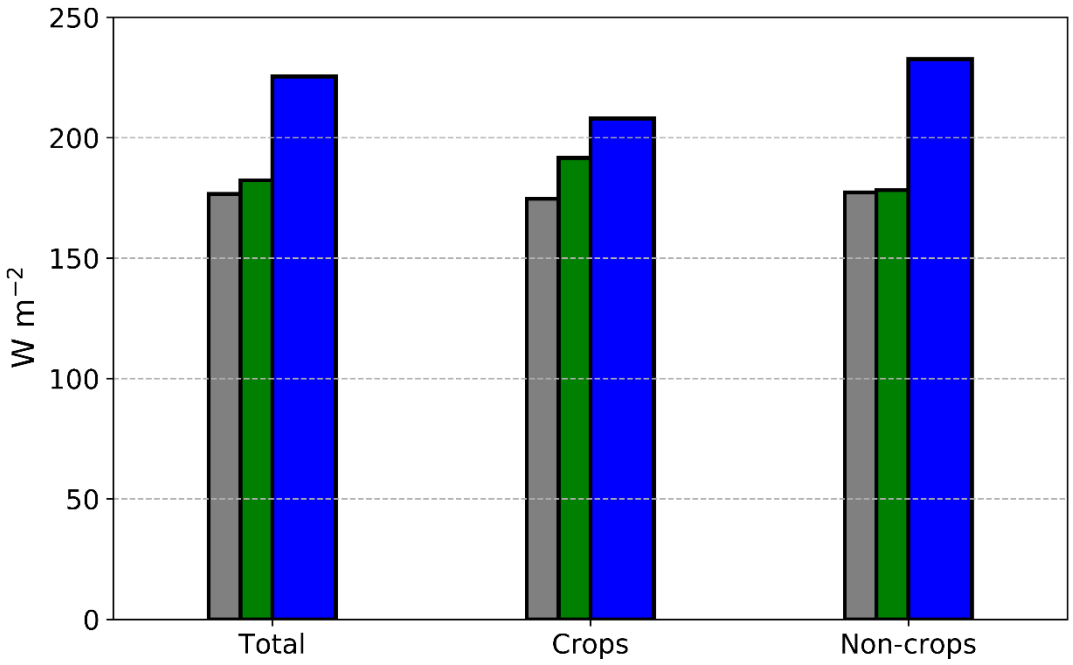

Figure S4. Average net radiation on the surface (W m^{-2}) in different regions.

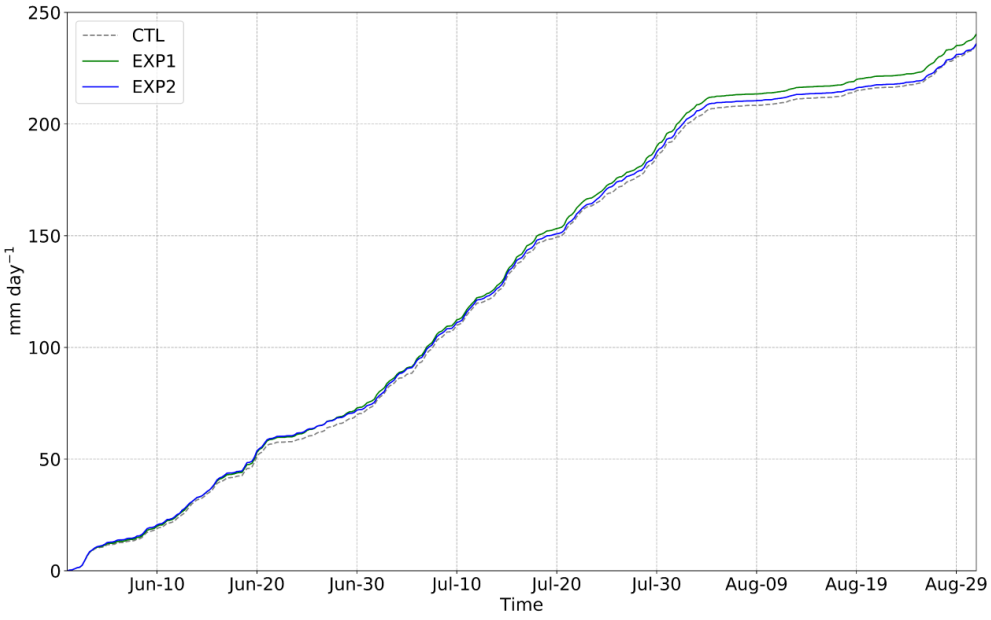

Figure S5. Time evolution of accumulated precipitation (mm day^{-1}) in summer of 2007. Grey, green, and blue correspond to CTL, EXP1, and EXP2 runs, respectively.